

Gating Kinetics of the α II T-Type Calcium Channel

CHARLES J. FRAZIER,¹ JOSE R. SERRANO,¹ ERIC G. GEORGE,¹ XIAOFENG YU,¹ AHALYA VISWANATHAN,¹ EDWARD PEREZ-REYES,² and STEPHEN W. JONES¹

¹Department of Physiology and Biophysics, Case Western Reserve University, Cleveland, OH 44106

²Department of Pharmacology, University of Virginia, Charlottesville, VA 22908

ABSTRACT The α II T-type calcium channel inactivates almost 10-fold more slowly than the other family members (α I and α H) or most native T-channels. We have examined the underlying mechanisms using whole-cell recordings from rat α II stably expressed in HEK293 cells. We found several kinetic differences between α I and α II, including some properties that at first appear qualitatively different. Notably, α II tail currents require two or even three exponentials, whereas α I tails were well described by a single exponential over a wide voltage range. Also, closed-state inactivation is more significant for α II, even for relatively strong depolarizations. Despite these differences, gating of α II can be described by the same kinetic scheme used for α I, where voltage sensor movement is allosterically coupled to inactivation. Nearly all of the rate constants in the model are 5–12-fold slower for α II, but the microscopic rate for channel closing is fourfold faster. This suggests that T-channels share a common gating mechanism, but with considerable quantitative variability.

KEY WORDS: inactivation • activation • T-current • LVA channel • kinetic models

INTRODUCTION

T-type calcium channels are important for the generation of repetitive activity in many neurons and other excitable cells (Huguenard, 1996). Several key features of T-channel kinetics underlie that functional role, notably activation and inactivation at unusually negative voltages, and more rapid and complete inactivation than most other calcium channels (Carbone and Lux, 1984). T-channels also close (deactivate) slowly upon hyperpolarization, which can allow maintained Ca^{2+} entry after repolarization (Armstrong and Matteson, 1985).

Although T-channels in native cells share many properties, there is evidence for kinetic and pharmacological diversity. Notably, T-channels of thalamic relay neurons inactivate rapidly ($\tau \sim 30$ ms above -30 mV; Coulter et al., 1989; Huguenard and McCormick, 1992), whereas T-channels of neurons in the reticular nucleus of the thalamus inactivate about threefold more slowly, and exhibit other detailed kinetic differences (Huguenard and Prince, 1992). These functional properties may contribute to the ability of reticular neurons to act as pacemakers for thalamic oscillations.

The cloning of three T-type calcium channels provided a basis for exploration of functional diversity among T-channels (Cribbs et al., 1998; Perez-Reyes et al., 1998; Lee et al., 1999). Two clones (α I and α H)

inactivate relatively rapidly ($\tau \sim 15$ ms above -30 mV), whereas the third (α II) inactivates almost 10-fold more slowly (Klößner et al., 1999; Kozlov et al., 1999; Lee et al., 1999; Monteil et al., 2000; McRory et al., 2001). Since α II is highly expressed in thalamic reticular neurons (Talley et al., 1999), it is a candidate for the kinetically unusual T-channel of those cells.

We recently examined in detail the gating kinetics of the α I T-type calcium channel at the level of whole-cell currents (Serrano et al., 1999). The results could be described by a model where inactivation and recovery are intrinsically independent of voltage, but coupled allosterically to voltage sensor movement. This is reminiscent of inactivation of Na^+ channels (Armstrong and Bezanilla, 1977; Kuo and Bean, 1994), although the structural basis of T-channel inactivation and its evolutionary relationship to other inactivation mechanisms is not known. One key feature of the model was relatively weak allosteric coupling between activation and inactivation, which made the macroscopic time constants for inactivation and recovery depend more weakly on voltage than commonly observed for voltage-dependent channels. Inactivation occurred primarily from the open state during brief, strong depolarizations, but long, weak depolarizations induced closed-state inactivation, strongly affecting the steady-state inactivation curve. Slow channel closing allowed some channels to inactivate (rather than deactivate) upon hyperpolarization, producing strong cumulative inactivation. Curiously, an accurate description of the kinetics at intermediate voltages required the postulate that only three of the four voltage sensors were coupled to the inactivation process (Serrano et al., 1999).

The present address of C.J. Frazier is Department of Pharmacology and Therapeutics, University of Florida, Gainesville, FL 32610.

Address correspondence to Stephen W. Jones, Department of Physiology and Biophysics, Case Western Reserve University, Cleveland, OH 44106. Fax: (216) 368-3952; E-mail: swj@po.cwru.edu

We report here a study of the kinetics of activation and inactivation of the α II T-type channel. The goal was to compare this slowly inactivating channel to the more typical α 1G T-channel. Can gating of α II be described by the same basic mechanism as α 1G, but with different parameters (e.g., a slower inactivation rate), or are there fundamental differences in the way these two channels respond to voltage?

MATERIALS AND METHODS

HEK293 cells stably expressing rat α II (GenBank accession No. AF086827) have been described previously (Lee et al., 1999). The sequence of that clone differs from the rat α II reported by McRory et al. (2001), leading to 32 differences in the deduced amino acid sequence. Eight of those differences occur in regions predicted to be membrane spanning. The most notable difference is the absence of three consecutive highly conserved amino acids in IIS4 of their clone, although discrepancies also exist in the S4 regions of repeat I and II. Our clone was resequenced, confirming the original sequence with three exceptions: W345 (not G), S1656 (not T), and P1737 (not A). Only one of these three sequences (W345) agrees with McRory et al. (2001). The coding region of both rat α II clones ends with the sequence TGLHPSCWGMT, whereas the human α II sequence reported by Monteil et al. (2000) contains an additional 157 amino acids at the COOH terminus. Examination of the human genomic sequence indicates that the rat α II results from alternative splicing of exon 33 to 34. The rat uses an internal splice site located 40 bp into exon 34, resulting in a change of the open reading frame. We have recently isolated a variant of rat α II that splices these exons in the same manner as the human, resulting in a much longer open reading frame with considerable homology to the human sequence.

The stably transfected HEK293 cells were grown in cell culture as described previously (Serrano et al., 1999). Currents were recorded in the whole-cell patch-clamp configuration using Axopatch 200A amplifiers and pClamp software (usually v. 8). The extracellular solution contained 140 mM NaCl, 2 mM CaCl₂, 1 mM MgCl₂, and 10 mM HEPES, adjusted to pH 7.2 with NaOH. The intracellular solution contained 120 mM NaCl, 11 mM EGTA, 1 mM CaCl₂, 4 mM MgATP, and 10 mM HEPES, pH 7.2 with NaOH. After titration, the estimated [Na⁺]_o was 144 mM and [Na⁺]_i = 160 mM. The estimated free [Ca²⁺]_i was 20 nM and [Mg²⁺]_i = 0.7 mM (Brooks and Storey, 1992). Series resistances were typically 3–9 M Ω , measured before compensation (nominally 80–95%). All experiments were performed at room temperature.

The holding potential was -100 mV. Except for some very long duration protocols (see Fig. 9), both “raw” currents and on-line leak-subtracted ($P/-4$) currents were recorded, and only leak-subtracted data are shown. Data were usually sampled at 20 kHz (or 10 kHz for some inactivation protocols where tail currents were not analyzed in detail), after analogue filtering at 25–50% of the sampling rate. It is noteworthy that some protocols required both high sampling rates and very long durations to accurately describe gating kinetics on different time scales (see Figs. 4 and 5 B). Data were analyzed primarily by Clampfit v. 8, although some analyses were done with Microsoft Excel or programs written locally in Visual Basic. Exponential fits were done with the Simplex or Levenberg-Marquardt methods of Clampfit v. 8, or (when parameters were constrained) using the Solver function of Excel to minimize the sum of squared errors. Values are given as means \pm SEM, and for figures showing averaged data, error bars \pm SEM are shown if larger than the symbol. Statistical significance levels given in the text are from paired two-tailed t tests (Excel), with $P < 0.05$ considered to be significant.

Kinetic models were simulated using SCoP v. 3.51 (Simulation Resources). Simulated data were either converted to binary files and analyzed by Clampfit, or imported into Excel.

RESULTS

Activation

Fig. 1 illustrates the primary protocols used to examine the kinetics of α II channels. Steps were given to voltages from -100 to $+70$ mV, either directly from -100 mV (Fig. 1 A) or after activation of the channels by 10-ms steps to $+60$ mV (Fig. 1 B). I-V relations measured from the two protocols are shown in Fig. 1 C. Channel activation was clearly detectable by -60 mV, and the peak inward current was near -30 mV. The instantaneous I-V relationship (Fig. 1 C, squares) was nonlinear, reflecting a high conductance to Ca²⁺ at negative voltages, a high conductance to Na⁺ at extreme positive voltages, but a lower conductance near the reversal potential. The reversal potential ($+21.4 \pm 1.3$ mV, $n = 5$) corresponds to a Goldman-Hodgkin-Katz permeability ratio $P_{Ca}/P_{Na} = 95$, compared with $P_{Ca}/P_{Na} = 150$ – 170 for α 1G (Serrano et al., 1999, 2000; calculated including Na⁺ used for titration, see MATERIALS AND METHODS).

The two I-V relationships in Fig. 1 C are the current at the time of peak activation at each voltage, and the instantaneous current after maximal activation (10 ms at $+60$ mV). At a given voltage, the driving force is the same, so the ratio of the two currents is the channel open probability (P_O)* relative to that at $+60$ mV. We use this “relative P_O ” ($P_{O,r}$) to assess the voltage dependence of channel activation (Fig. 1 D). A fit of this activation curve to a single Boltzmann relation missed the data points at the foot of the curve (Fig. 1 D, dashed curve), whereas a Boltzmann raised to the fourth power described the data somewhat more accurately (Fig. 1 D, solid curve). The activation curves for α 1G and α II do not have precisely the same shape, but the point of 50% activation was ~ 20 mV more positive for α II.

The protocols of Fig. 1 (A and B) were also used to measure the time dependence of channel gating. Fig. 2 illustrates tail currents from Fig. 1 B on a much faster time scale. Over the range of voltages where channels deactivate significantly, the tail currents were not well described by single exponentials, but the sum of two exponentials could fit the data well (Fig. 2). Although only 10 ms is shown in Fig. 2, the currents were fitted over the entire 50-ms pulse duration (Fig. 1 B). The fitted time constants are shown in Fig. 3. Especially at more negative voltages, the fast component was the largest (62–72% of the total from -100 to -60 mV, with 27–38% slow and 0–6% constant). Biexponential

*Abbreviations used in this paper: P_O , open channel probability; $P_{O,r}$, P_O relative to that produced by a 10-ms depolarization from -100 to $+60$ mV.

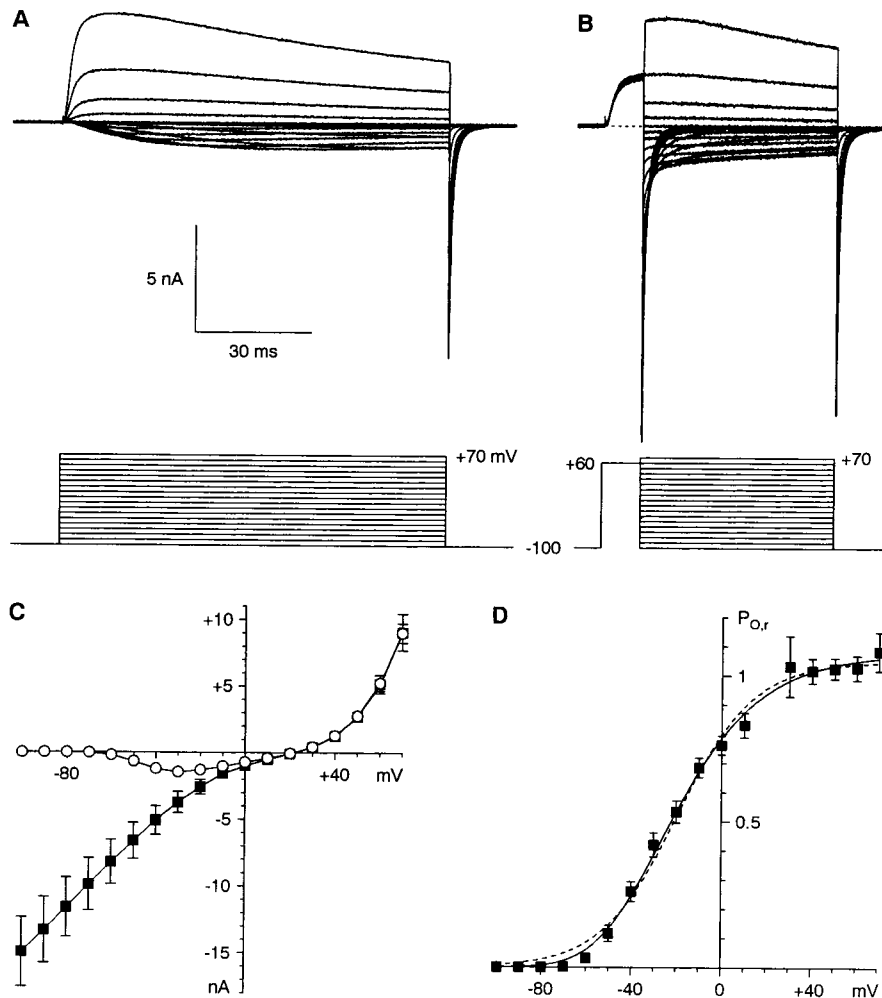


FIGURE 1. Protocols for activation kinetics. (A) Activation upon direct depolarization from -100 mV. 100-ms steps are shown here, but 500-ms steps were used for all analysis. (B) The protocol used for measurement of the instantaneous I-V relationship, and for the kinetics of tail currents. Tail currents are illustrated on a faster time scale in Fig. 2. A and B are from cell 99622; 5-kHz Gaussian filter. (C) I-V relations were measured at the time of maximal current during 500-ms steps with the protocol of A (open circles) or at the time of peak tail current for B (solid squares). (D) The activation curve measured from the ratio of the two I-V curves in C ($P_{O,r}$). The ratio is not shown at $+20$ mV, which is very close to the reversal potential. The dashed curve is a fit to a single Boltzmann relation ($V_{1/2} = -19.5$ mV, e-fold for 16.8 mV, maximal ratio 1.05). The solid curve is a fit to a Boltzmann raised to the fourth power ($V_{1/2} = -58.9$ mV, e-fold for 23.5 mV, maximal ratio 1.02). That $V_{1/2}$ reflects the activation of each voltage sensor, not the entire channel. Data in C and D are averages from five cells.

tails were also observed in the absence of Mg^{2+} , so this does not result from time-dependent block by Mg^{2+} (Serrano et al., 2000). We also considered whether the fast component of the tail current might be a gating current. After leak subtraction, a small transient outward current was visible near the reversal potential with the protocol of Fig. 1 A, with integrated amplitude of 0.22 ± 0.06 pC, only $6 \pm 1\%$ of the integrated fast component of the tail current (4.1 ± 0.7 pC, $n = 5$).

We previously described $\alpha 1G$ tail currents as monoexponential, but noted that fitting to the sum of two exponentials often yielded a small, fast component (Serrano et al., 1999), with relative amplitude $\sim 20\%$. In contrast to $\alpha 1I$ (where the relative amplitude of the fast component was much larger), gating currents and/or Mg^{2+} block could account for much of the fast component of $\alpha 1G$. Thus, we conclude that a single exponential provides an adequate description of tail currents for $\alpha 1G$ but not $\alpha 1I$.

The time constants at the most negative voltages should be interpreted with caution, as the fitted values varied significantly with the series resistance and clamp

speed. For the tail current analysis in Figs. 2–3, cells were selected for fast clamp, where the time to peak of the tail current was 0.35 ms or less. When the voltage clamp was slower, tail currents occasionally appeared to be monoexponential at -100 mV, as expected from RC filtering of the faster component by the electrode, but were still clearly biexponential at less negative voltages (-80 to -20 mV). The voltage-clamp error is largest at the most negative voltages, as the tail currents are larger and faster.

Envelope Test

The large, slowly inactivating currents observed at strongly depolarized voltages (Fig. 1, A and B) look very different from classical T-currents, and could potentially reflect contaminating currents through channels endogenous to HEK 293 cells. To evaluate that, we used the “envelope test,” where the current during a maintained depolarization is compared with the tail currents measured after voltage steps of different duration (Fig. 4, A and B). The initial tail current amplitudes, scaled to account for the difference in driving

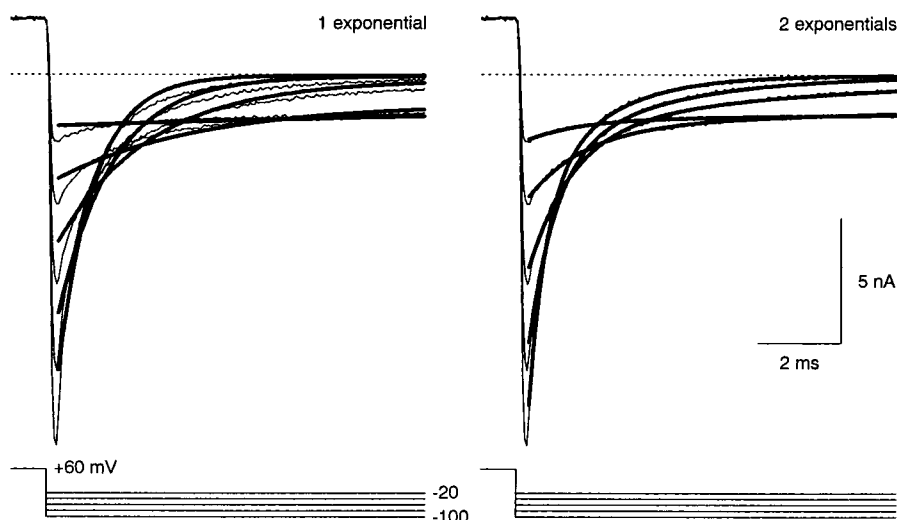


FIGURE 2. Exponential fits to tail currents. Records are from Fig. 1 B on an expanded time scale. The thicker smooth curves are fits to a single exponential (left) or the sum of two exponentials (right), beginning 0.35 ms after repolarization from +60 mV.

force, superimpose upon the currents measured during depolarization, for steps to either -20 or $+60$ mV. Notably, the time course for inactivation was the same, measured either directly from the current during depolarization, or indirectly from the envelope of tail cur-

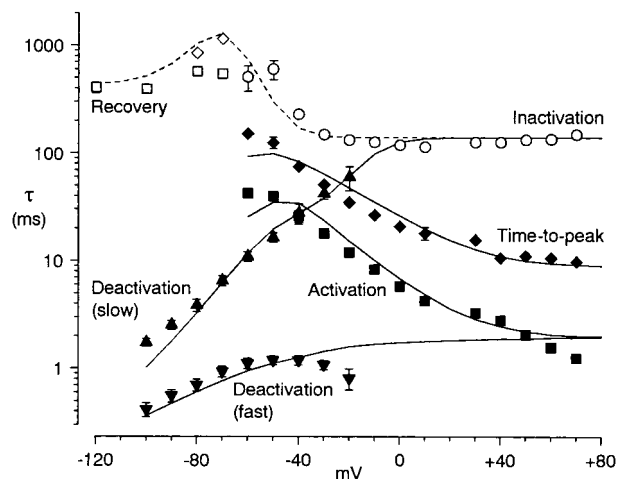


FIGURE 3. Time constants for activation and inactivation. Data points are experimental measurements ($n = 4-8$, except $n = 3$ at $+70$ mV). The lines are from the kinetic model presented in Figs. 12 and 13 calculated in 10-mV intervals. Activation kinetics are shown with solid symbols and lines; inactivation with open symbols and dashed lines. Three measurements are from the protocol of Fig. 1 A (with 500-ms steps): activation time constants (solid squares), measured from the rising phase of the current, from ~ 10 to 90% of the peak; time to peak (solid diamonds); and inactivation (open circles), fitted starting shortly after the peak. The fast and slow components of deactivation were measured from biexponential fits to tail currents from the protocol of Fig. 1 B. The time course of recovery from inactivation (open squares) and of development of inactivation at -70 and -80 mV (open diamonds) are from single exponential fits from the protocol of Fig. 8, allowing different time constants for inactivation and recovery at each voltage.

rents. This is consistent with both inward and outward currents flowing through the same population of channels. It also suggests that the large currents observed during long voltage steps used did not produce significant changes in ion concentrations, which can occur in small cells (Frazier et al., 2000).

With the envelope protocol, tail currents at -100 mV were also described by the sum of two exponentials (Fig. 4, C and D). As the pulse length increased, the time constants could be constrained to remain constant, but the relative amplitude of the slow component increased, from 0.12 ± 0.02 after 10 ms to 0.44 ± 0.05 after 1 s at $+60$ mV ($n = 4$; similar effect at -20 mV). Note that the two largest tail currents cross over in Fig. 4 C. Slower tail currents after partial inactivation have been reported previously for $\alpha 1I$ (Warre and Randall, 2000). As Warre and Randall (2000) noted, this result is the opposite of the effect of series resistance error, which would slow the kinetics of larger tail currents.

Activation, Deactivation, and Inactivation

Fig. 3 summarizes several measurements of the time course of activation and inactivation, primarily from the protocols of Fig. 1 (measurement of the time course of inactivation and recovery at more negative voltages is described below). One noteworthy feature is that macroscopic inactivation is much slower than activation or deactivation at extreme voltages, but at intermediate voltages (e.g., -40 mV), activation and inactivation kinetics are less clearly separated. We examined the time course of currents in this voltage region more thoroughly.

Upon repolarization, the open channel can either close (deactivate) or inactivate. Thus, the simplest interpretation of the biexponential decay of tail currents (Figs. 2-4) is that the fast and slow components reflect

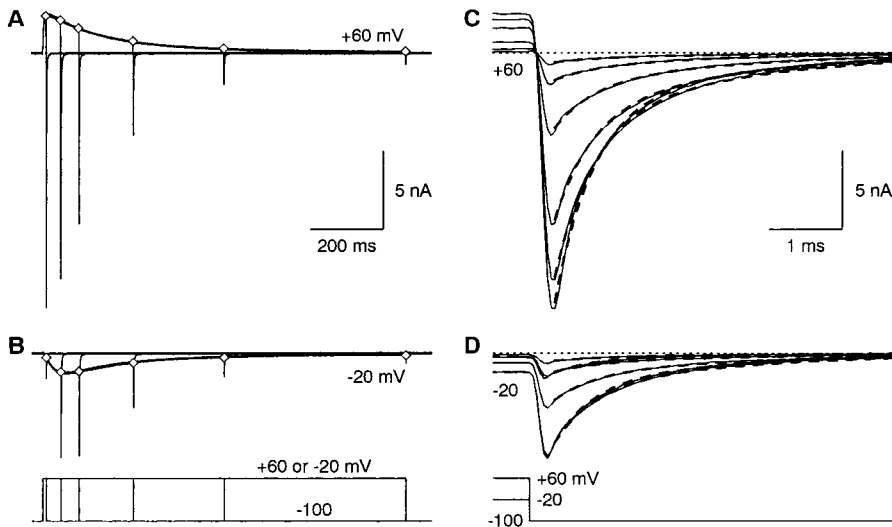


FIGURE 4. Envelope test for current isolation. Voltage steps lasting 10, 50, 100, 250, 500, or 1000 ms were given to +60 mV (A) or -20 mV (B). The open diamonds are the peak tail currents, scaled to correct for driving force. The scaling factor was the sum of the currents at the end of the six steps divided by the sum of the six corresponding tail currents. Cell 99622; 4-kHz Gaussian filter. (C-D) Superimposed tail currents on a 200-fold expanded time scale. The dashed curves are fits to the sum of two exponentials, from 0.35 to 20 ms after repolarization from +60 mV. The time constants were constrained to be the same for all records shown (0.53 and 2.34 ms), with variable amplitudes.

deactivation and inactivation, respectively. We assessed that by comparing the time course of turn-on and turn-off of the current, measured at the same voltage (Fig. 5). In principle, the time course of currents at any voltage should be described by the sum of exponentials, with the time constants depending only on voltage, and

the relative amplitudes of the components depending also on the initial conditions. Thus, we constrained the time constants to be the same for the currents recorded as the channels turn on or turn off (Brown et al., 1983).

Upon weak depolarization, channels activated slowly after a clear delay, with time to peak as slow as 100 ms

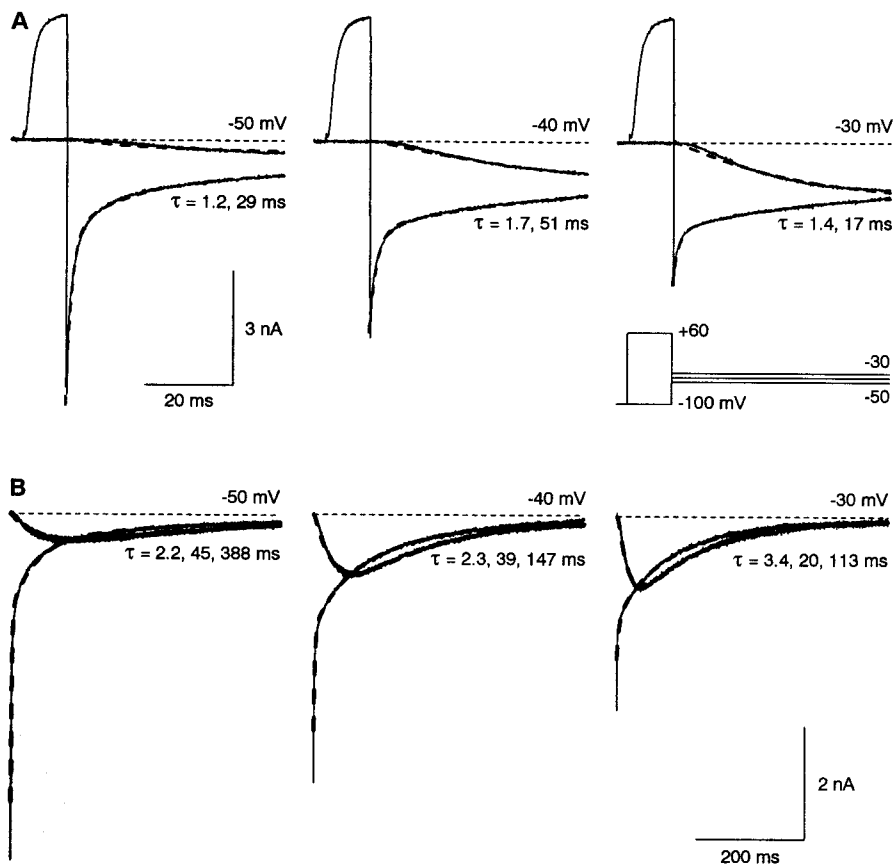


FIGURE 5. Kinetics of activation, deactivation, and inactivation at intermediate voltages. (A) Records extracted from the protocols of Fig. 1 A-B. The dashed curves are fits to the sum of two exponentials, with the two time constants constrained to be the same at each voltage. Without further constraints, the fit to the time course of activation was often biphasic (an initial outward current followed by inward current), which is not physically realistic. Therefore, for activation, the initial amplitude and rate of rise (dI/dt) at $t = 0$ were constrained to be ≤ 0 . Cell 99711; 4-kHz Gaussian filter. (B) Records from a similar protocol in a different cell (00d07), but with longer (500 ms) steps to -50 to -30 mV. In each panel, one record is the tail current after repolarization from +60 mV (for 20 ms), and two records are for direct depolarization from -100 mV to the indicated voltage, recorded before and after the tail current (as a control for rundown). The currents cross over because inactivation begins earlier with the tail protocol, as some inactivation occurs during the step to +60 mV, and during the initial portion of the tail current. The dashed curves are fits to the sum of three exponentials, with the same three time constants for all records at each voltage. 3-kHz Gaussian filter, with 0.3 ms blanked.

(Fig. 3). The slow time course of activation was mirrored by the slow component of deactivation (Fig. 5 A). Indeed, the time course of both activation and deactivation could be approximated by the sum of two exponentials, although the delay before activation was not well described (suggesting that the channel passes through more than two closed states before opening). The slower time constant was roughly similar to those found by fitting the tail current or the activation time course separately, and was considerably faster than the time constant of inactivation measured during long depolarization (110–500 ms; Fig. 3). This suggests that the two tail current time constants (measured during 50-ms steps) both primarily reflect the kinetics of the activation process.

In the voltage range where channels activate significantly, the biexponential fits to tail currents included a relatively large constant component (16–25% from -50 to -20 mV; see also Fig. 5 A). That is not realistic, as currents eventually inactivate almost completely in that voltage range (see Fig. 7). This led us to examine currents during steps lasting several hundred milliseconds. That revealed a third exponential component, corresponding to inactivation (Fig. 5 B). When the currents were fitted to the sum of three exponentials at each voltage, the time constants corresponded approximately to those found for fast deactivation, slow deactivation (or activation), and inactivation in Fig. 3.

The three exponential components were most clearly demonstrated in tail currents at -40 mV (Fig. 6), where the time constants were well separated, and the amplitudes were comparable and thus easily detectable. In seven cells, the time constants were 1.5 ± 0.2 , 27 ± 4 , and 118 ± 14 ms, with relative amplitudes 0.34 ± 0.04 , 0.20 ± 0.01 , and 0.43 ± 0.03 , respectively (offset 0.026 ± 0.004), including three cells examined with no Mg^{2+} .

The time constants from these unconstrained three-exponential fits did not agree precisely with those from the simultaneous fits to turn-on and turn-off kinetics. In particular, the fast time constant was generally smaller for the fits to turn-off kinetics alone (compare Fig. 6 with Fig. 5 B, middle). By eye, the simultaneous fits missed

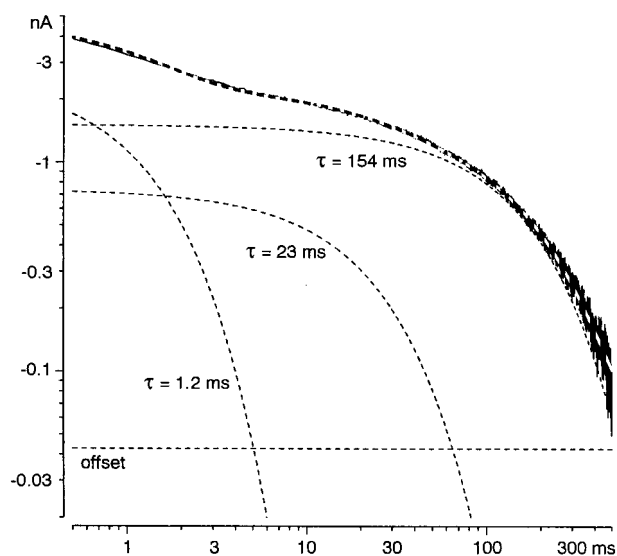


FIGURE 6. Three components of tail currents at -40 mV, shown on a log-log scale. The data record is from the middle panel of Fig. 5 B. The dashed curves are the three fitted exponential components, the offset, and the sum of all components.

part of the fast tail current, and underestimated the delay in activation. Also, in two out of four cells, the slow time constant at -50 mV was about threefold larger for the simultaneous fits (Fig. 5 B, left). This suggests that a full description of α II kinetics would require more than three exponential components in this voltage region. Our main conclusion from this analysis is that there are at least three components, with time constants on the 1-, 10-, and 100-ms time scales.

Complex tail current kinetics are not unexpected, as both deactivation and inactivation can contribute, on different time scales. However, the observation of bi- or triexponential tail currents for α II contrasts sharply with α 1G, where tail currents could be described well by a single exponential (Serrano et al., 1999).

Inactivation

To examine the voltage dependence of inactivation, we first gave long depolarizations (1.5 s) to a range of volt-

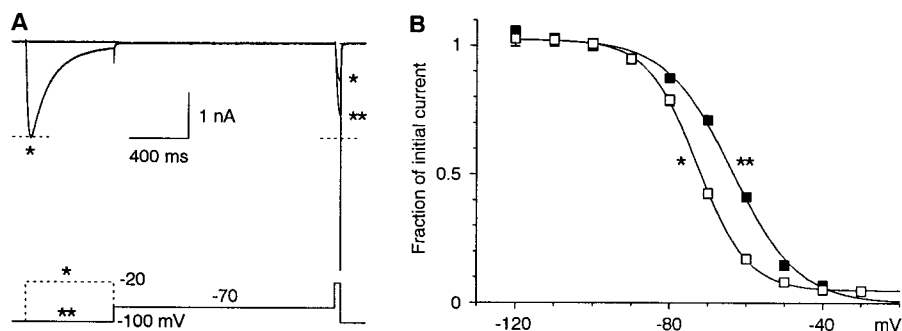


FIGURE 7. The voltage dependence of inactivation measured at 1.5 s. (A) Illustration of the protocols, for steps to -70 mV, near the midpoint of the inactivation curve. The cell was stepped to -70 mV either directly (**), or after a 0.6-s step to -20 mV (*). Note that the extent of inactivation measured by the subsequent test pulse was strongly affected by the step to -20 mV. Cell 99715; 1-kHz Gaussian filter. (B) Inactivation measured for steps directly from -100 mV (**, open squares), or after prior inactivation at -20 mV (*, solid squares). Data are from three cells where both protocols were run. The curves are fits to single Boltzmann ($V_{1/2} = -72.8$ mV, e-fold for 6.5 mV, amplitude = 0.98, and offset = 0.05; $V_{1/2} = -63.7$ mV, e-fold for 8.7 mV, amplitude = 1.03, and offset = 0).

ages, followed by brief test pulses to -20 mV (Fig. 7, protocol marked by two asterisks). The measured inactivation curve was well described by a single Boltzmann, with midpoint -64 mV. To determine whether that inactivation curve truly represented steady-state inactivation, we used the same protocol, except that channels were initially inactivated by 90% by a 0.6-s step to -20 mV. At steady state, the extent of inactivation should depend only on the conditioning voltage, and should be independent of the initial conditions. The data were again well described by a Boltzmann, but with a midpoint of -73 mV. This demonstrates that 1.5 s is not long enough to reach steady state, in contrast to our result with $\alpha 1G$ (Serrano et al., 1999).

To further explore the time and voltage dependence of inactivation, we compared the time course of inactivation and recovery at several voltages, using steps up to 3 s (Fig. 8). Instead of achieving steady state, longer voltage steps revealed a second component of inactivation. When inactivation and recovery were fitted separately to single exponential functions at -70 or -80 mV, the time constant for recovery was significantly faster (Fig. 3, open squares versus open diamonds). When inactivation and recovery were constrained to have the same time constant, single exponentials did not fit very well (Fig. 8, dashed lines). Note that the single exponentials predict more rapid convergence of inactivation and recovery than observed at -70 mV. At -60 mV, where only recovery was tested with this protocol, there was a small but clear initial recovery phase, followed by subsequent development of additional inactivation. These results are not consistent with a single inactivation process, and suggest that voltage steps longer than 1 s begin to evoke a slow inactivation process. The nonmonotonic time course of recovery from inactivation at -60 mV could be explained if the slower inactivation process is more complete at that voltage.

Additional protocols were used to further demonstrate slow inactivation. Fig. 9 A compares the time course of inactivation versus recovery at -70 mV for steps lasting up to 9 s. Inactivation continued to develop over several seconds, whereas recovery was maximal at 1–3 s. With the recovery protocol, channel availability at 9 s was $80 \pm 5\%$ of that at 3 s ($n = 6$; $P = 0.008$). Because of slow inactivation, even 9 s was not long enough to completely reach steady state, as currents measured at 9 s with the recovery protocol were $85 \pm 3\%$ of those measured with the inactivation protocol ($n = 6$; $P = 0.005$). The time course could be fitted to the sum of two exponentials, with $\tau = 0.73 \pm 0.03$ s and 4.7 ± 0.8 s, with $75 \pm 5\%$ inactivation ($n = 6$).

When test pulses were given while the holding potential was changed from -100 to -80 or -70 mV, two components of inactivation were again visible (Fig. 9 C). Recovery from inactivation was essentially complete

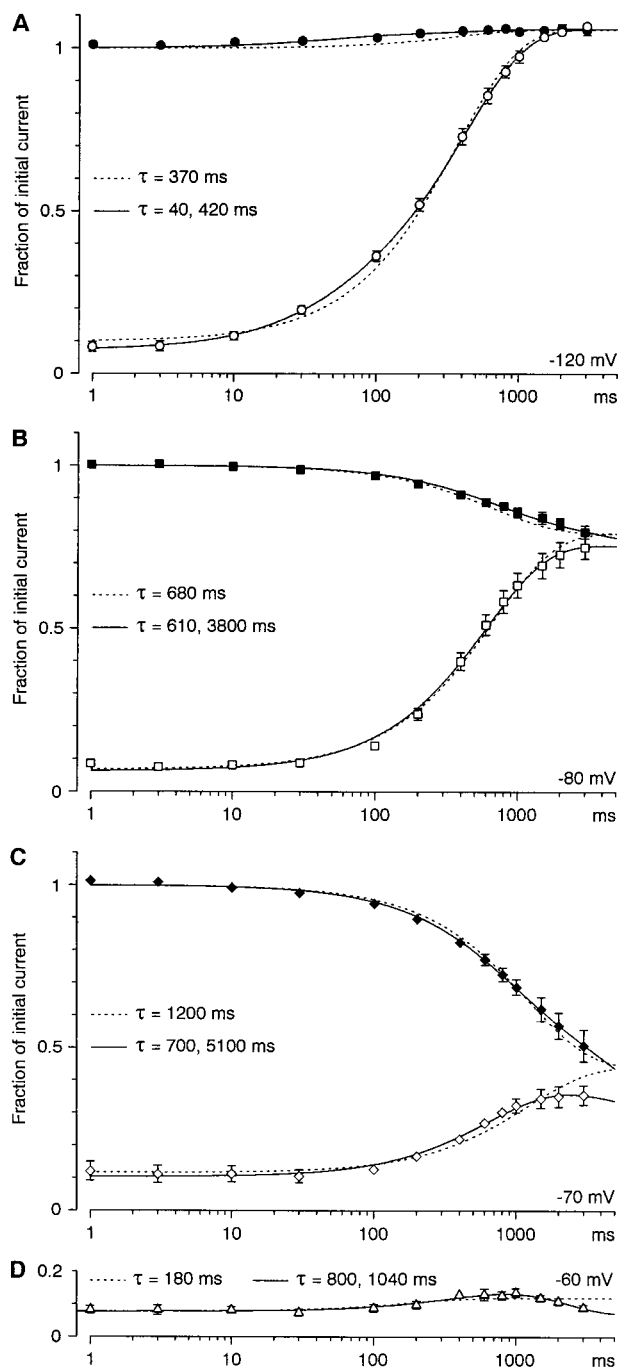


FIGURE 8. The time course of development of inactivation (solid symbols) and recovery from inactivation (open symbols). Protocols were as in Fig. 7, except that the duration at each voltage was varied from 1 ms to 3 s ($n = 4-7$, except $n = 3$ at -60 mV). Dashed curves are fits to single exponentials, with a single time constant for inactivation and recovery at each voltage. Solid curves are fits to the sum of two exponentials, with the same two time constants at each voltage for both recovery and for development of inactivation, except at -60 mV, where only recovery was examined. The longer time constants may not be accurate, as they are comparable to the duration of the protocol.

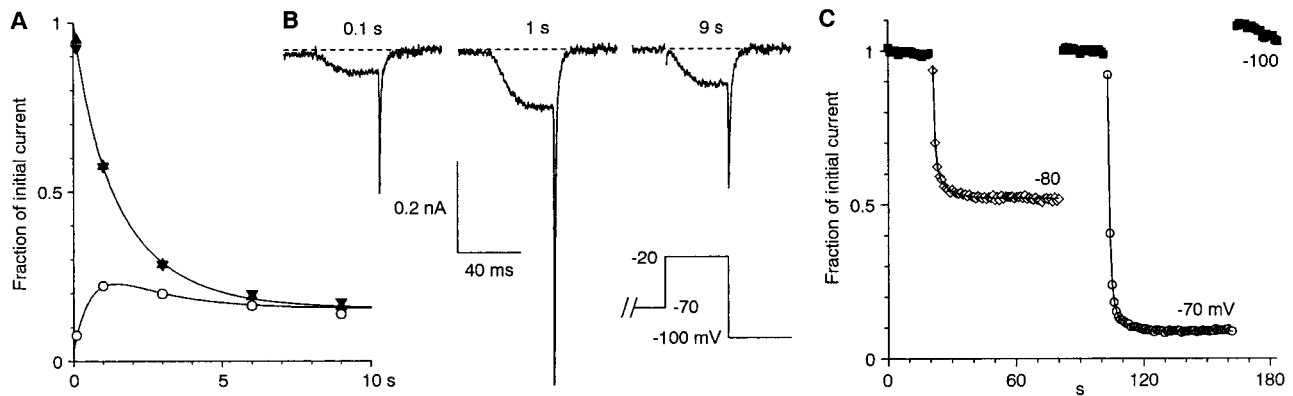


FIGURE 9. Slow inactivation of α II. (A) Comparison of inactivation and recovery, as in Fig. 8, but for up to 9 s at -70 mV. For each duration, three measurements are shown since the inactivation protocol was given twice, before and after the recovery protocol, as a control for rundown or accumulation of inactivation. Currents were normalized to the inactivating pulse from the recovery protocol (0.6 s at -20 mV). The smooth curves are fits to the sum of two exponentials ($\tau = 0.63$ s and 2.0 s), with extrapolated steady-state inactivation of 84%. The extent of inactivation was somewhat greater than average in this cell (compare also the 3-s time points to Fig. 8). These voltages are near the midpoint of the inactivation curve, so small voltage offsets would have a large effect on the observed inactivation. (B) Sample records from the recovery protocol of the experiment shown in A for the indicated durations. Note that recovery was maximal at 1 s, with further inactivation developing at later times. Because of the long durations used, currents were leak-subtracted off line, using 50-ms steps from -100 to -120 mV. Cell 01403; 1-kHz Gaussian filter. For the record at 9 s, 1 ms was blanked at the onset of the step to -20 mV. (C) Time course of inactivation measured at -80 and -70 mV, in the same cell as A and B. Test pulses to -20 mV were given every 1 s from a holding potential of -100 (solid squares), -80 (open diamonds), or -70 mV (open circles). At -70 or -80 mV, the first test step was given 0.1 s after the change in holding potential. At -100 mV, the first test step was given 2 s later. The solid curves through the data at -80 and -70 mV are fits to the sum of two exponentials ($\tau = 0.77$ s and 6.1 s at -80 mV, with relative amplitudes 0.37 and 0.11 respectively; $\tau = 0.87$ s and 5.6 s at -70 mV, amplitudes 0.79 and 0.12). Measurements were not leak-subtracted, and were normalized to the average of the values recorded during the second interval at -100 mV (after -80 mV, before -70 mV).

in the 2 s interval between the last pulse from -80 or -70 mV and the first test pulse from -100 mV.

Although these experiments do not fully characterize the kinetics of the slow inactivation process, they are sufficient to demonstrate its existence. For our purposes here, the main point is that the slow inactivation process interfered with direct measurement of steady-state inactivation for α II.

State Dependence of Inactivation

For α 1G, inactivation occurred primarily from open states at more depolarized voltages, but primarily from closed states near the midpoint of the inactivation curve (Serrano et al., 1999). Closed-state inactivation also dominated at more negative voltages for α II (Fig. 10). The amount of open-state inactivation was “predicted” (Bean, 1981; Serrano et al., 1999) by:

$$P_I = \sum k_I P_{O,r}(t) \Delta t, \quad (1)$$

where P_I is the predicted probability that the channel will become inactivated, k_I is the rate constant for inactivation (determined from the time constant for inactivation at depolarized voltages), and $P_{O,r}$ is calculated as in Fig. 1 D for each data point. This calculation assumes that open-state inactivation is “absorbing” which would overestimate open-state inactivation and voltage-independent. Considerable inactivation occurred both at -80

mV, where there was no detectable channel opening and, thus, no predicted open-state inactivation, and at -70 mV, where channel opening was barely detectable (Fig. 10). This demonstrates that inactivation can occur

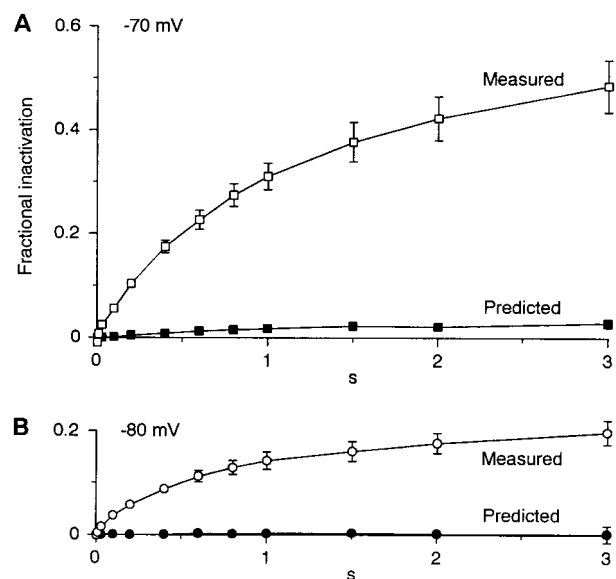


FIGURE 10. Test for closed-state inactivation at -70 (A) and -80 mV (B). The measured inactivation data (open symbols) are from Fig. 8. Predicted open-state inactivation (closed symbols) was calculated from the integrated $P_{O,r}$ and the inactivation rate (at -20 mV) using Eq. 1. At -70 mV, $n = 5-6$; at -80 mV, $n = 4$.

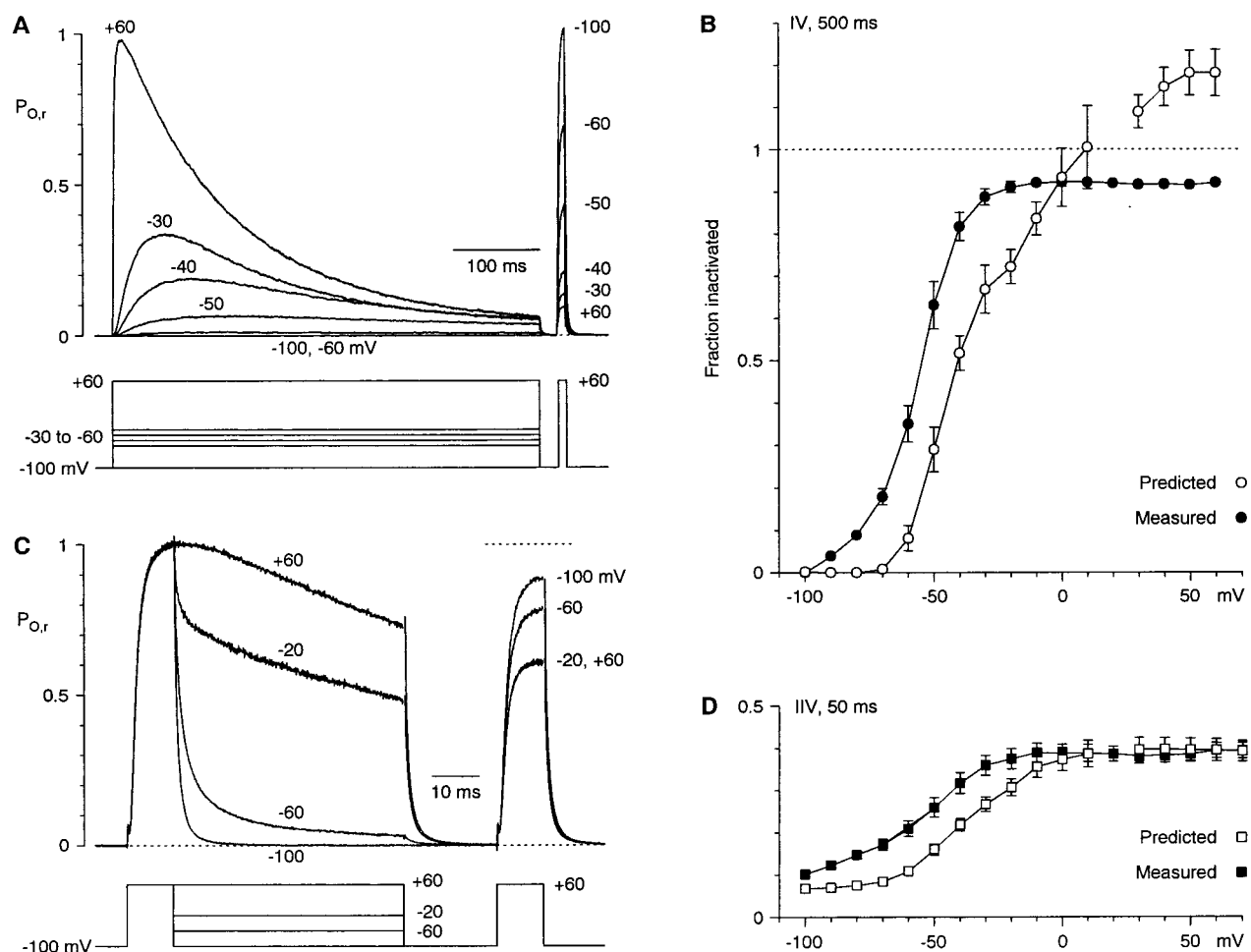


FIGURE 11. Test for closed-state inactivation at more positive voltages. (A) Currents recorded with the indicated protocol were converted to $P_{O,r}$ using the instantaneous I-V relationship measured in the same cell. Only selected voltage steps are shown. Cell 99711; 1-kHz Gaussian filter. (B) Inactivation from the protocol of A. Measured inactivation was from the test pulses at the right in A; predicted open-state inactivation was calculated using Eq. 1. (C) $P_{O,r}$ during the instantaneous I-V protocol of Fig. 1 B, followed by test pulses to +60 mV. Cell 99711; 3-kHz Gaussian filter. (D) Measured and predicted inactivation from the protocol of C. Data in B and D are averaged from the same five cells.

directly from closed states for α II, and that closed-state inactivation dominates at the more negative voltages.

The state dependence of inactivation at more depolarized voltages was examined with the protocols of Fig. 1, including test pulses to +60 mV to assess inactivation (Fig. 11). The recorded currents were converted to $P_{O,r}$, to allow visual evaluation of the correlation between channel opening and inactivation. 500-ms voltage steps to -60 or -50 mV opened few channels, but induced considerable inactivation (Fig. 11 A). Steps to +60 mV produced about twice as much integrated $P_{O,r}$ than steps to -30 mV, but the extent of inactivation was comparable (Fig. 11, A and B). This suggests that about half of the inactivation at -30 mV must have occurred from closed states. The measured inactivation exceeds the predicted open-state inactivation from -90 to -10 mV (Fig. 11 B).

Closed-state inactivation can be demonstrated even for relatively brief depolarizations with the protocol of

Fig. 1 B (see also Fig. 11, C and D). With an interpulse voltage of -100 mV, two 10-ms steps to +60 mV separated by 70 ms produced $10 \pm 1\%$ inactivation ($n = 5$). Considerably more inactivation occurred at -60 mV ($21 \pm 2\%$), even though the integrated $P_{O,r}$ was only slightly greater. $P_{O,r}$ is clearly lower at -20 mV than at +60 mV, because a significant fraction of channels deactivate at -20 mV (Fig. 11 B), as expected from the activation curve (Fig. 1 D). However, the extent of inactivation was indistinguishable at -20 and +60 mV ($37 \pm 2\%$ vs. $39 \pm 2\%$, respectively). This implies that closed-state inactivation is significant even at -20 mV. Furthermore, the net rate of inactivation must be the same at -20 and +60 mV, despite the difference in $P_{O,r}$. That is also shown by the time constants for inactivation, which are essentially constant above -30 mV (Fig. 3). Thus, certain closed states, presumably those close to the open state, inactivate as rapidly as the open state itself.

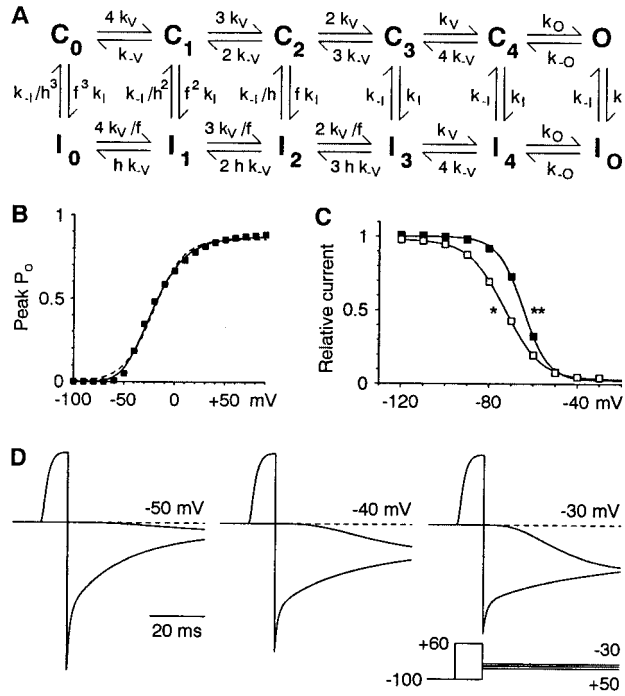


FIGURE 12. A kinetic model for gating of α II T-type calcium channels. (A) The kinetic scheme (Serrano et al., 1999). The model is defined by 11 parameters: 6 rate constants at 0 mV, 3 voltage dependences, and 2 allosteric factors (Table I). (B) Activation curve. Solid symbols are calculated from the model. The dashed curve is a fit to a single Boltzmann relation ($V_{1/2} = -21.1$ mV, e-fold for 14.7 mV, maximal $P_{O,r} = 0.86$). The solid curve is a fit to a Boltzmann raised to the fourth power ($V_{1/2} = -55.0$ mV, e-fold for 19.9 mV, maximal $P_{O,r} = 0.97$). (C) Voltage dependence of inactivation. Data points were measured from simulations using the protocols of Fig. 7 (solid squares, without prepulse to -20 mV; open squares, with prepulse). The curves are fits to a single Boltzmann (for recovery, $V_{1/2} = -72.9$ mV, e-fold for 8.2 mV, amplitude = 0.95, and offset = 0.03; for inactivation, $V_{1/2} = -64.7$ mV, e-fold for 5.8 mV, amplitude = 0.98, and offset = 0.02). (D) Comparison of the kinetics of activation and deactivation, as in Fig. 5 A. Currents (arbitrary units) were calculated assuming a linear instantaneous I-V relationship with a reversal potential of +25 mV.

Completeness of Inactivation

Inactivation of α II is incomplete, on the time scale examined. For the longest steps given with the envelope protocol (Fig. 4), $P_{O,r}$ after 1 s at -20 mV was 0.021 ± 0.006 (measured at the end of the depolarizing step) or 0.036 ± 0.008 (from the tail currents); at $+60$ mV, corresponding values were 0.032 ± 0.006 and 0.033 ± 0.007 ($n = 4$). From single exponential fits to those records, the time constants for inactivation were 165 ± 14 ms at $+60$ mV, and 167 ± 16 ms at -20 mV, with offsets of 0.032 ± 0.005 and 0.023 ± 0.005 , respectively. If inactivation occurred at the measured rate and was fully absorbing, the residual $P_{O,r}$ at 1 s would be only 0.003 ± 0.001 at $+60$ mV and 0.003 ± 0.002 at -20 mV. Thus, fast inactivation spares $\sim 2\%$ of α II channels at steady state, over a wide voltage range, as previously ob-

served for α IG (Serrano et al., 1999). Incomplete inactivation is also visible in Fig. 11 A, where inactivation at $+60$ mV was fitted with $\tau = 130$ ms and an offset of $P_{O,r} = 0.05$ (on average, $\tau = 134 \pm 9$ ms with offset 0.037 ± 0.005 , $n = 5$). That caused the predicted inactivation to exceed 1.0 at the most depolarized voltages (Fig. 11 B).

Kinetic Model

We described gating of α II using the same kinetic scheme proposed for α IG (Fig. 12 A and Table I). Briefly, the model assumes a linear pathway for activation (voltage sensor movement followed by channel opening), with inactivation allosterically coupled to the first three voltage sensors to activate (Serrano et al., 1999). Some of the model parameters were determined rather directly from the data, and were clearly different from α IG. The inactivation rate (k_I) was determined from the time constant for inactivation at depolarized voltages (Fig. 3), and the reverse rate (k_{-I}) from the extent of inactivation. Given those values, the allosteric factor for recovery (h) fixed the limiting rate of recovery from inactivation at negative voltages. The channel opening (k_O) rate limits the rate of activation at positive voltages. The charge movement associated with voltage sensor movement (and with channel closing) was kept the same as for α IG. The other four parameters (k_V , k_{-V} , k_{-O} , and f) were not directly determined, and were adjusted to describe the activation curve (Fig. 12 B), inactivation curve (Fig. 12 C), activation and deactivation time constants, and current time to peak (Fig. 3). The kinetics of activation for weak depolarizations (Fig. 12 D) was strongly affected by the speed of voltage sensor movement, such that twofold changes in k_V and k_{-V} produced activation that was clearly too fast or too slow. The model also produced a considerable amount of closed-state inactivation. The measured inactivation ex-

TABLE I
Comparison of Model Parameters for α II and α IG

Parameter	α II	α IG	Ratio (α IG/ α II)
k_V	200 s^{-1}	$2,500 \text{ s}^{-1}$	12.50
k_{-V}	1.5 s^{-1}	8 s^{-1}	5.33
k_O	500 s^{-1}	$4,000 \text{ s}^{-1}$	8.00
k_{-O}	100 s^{-1}	25 s^{-1}	0.25
k_I	7 s^{-1}	70 s^{-1}	10.00
k_{-I}	0.21 s^{-1}	1.4 s^{-1}	6.67
f	0.2	0.2	1.00
h	0.45	0.5	0.90

The kinetic scheme is illustrated in Fig. 12 A. Rate constants are at 0 mV. Three rates are voltage dependent, k_V , k_{-V} , and k_{-O} , with associated charge of +1.0, -1.39 , and -0.74 , respectively, for both channels. The allosteric factors f and h are unitless. Parameters for α IG are from Serrano et al. (1999).

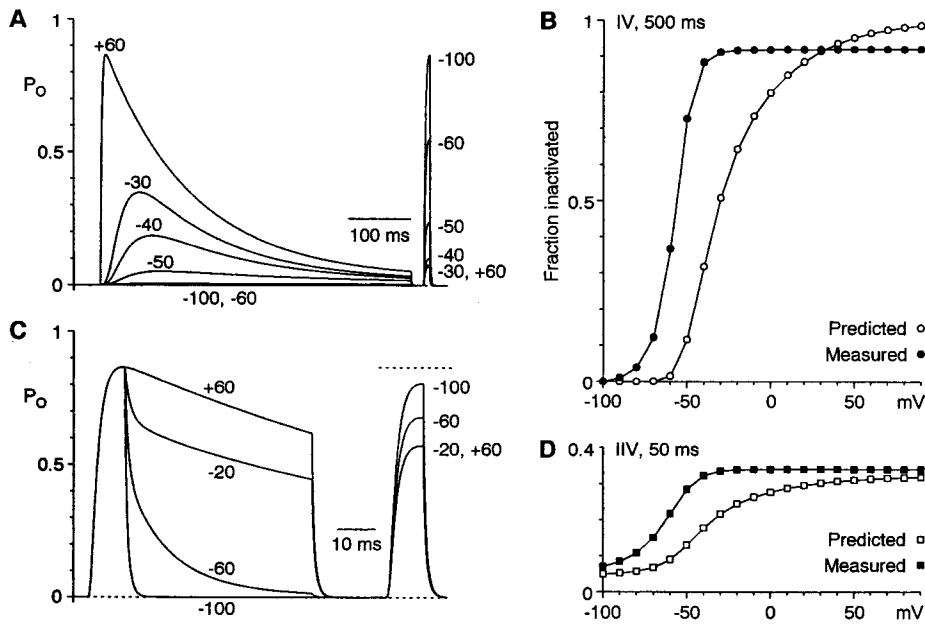


FIGURE 13. Measured inactivation versus predicted open-state inactivation for the model of Fig. 12 A. The protocols, calculations, and arrangement of the panels are as in Fig. 11, except that $P_{O,r}$ is shown rather than $P_{O,r}$.

ceeded the predicted open-state inactivation (Fig. 13), much as observed experimentally (Fig. 11).

Table I shows that most rates are 5–12-fold slower for α II, compared with α IG. But the kinetics of α II are not simply scaled with respect to α IG, since one crucial rate is actually fourfold faster for α II (channel closing, k_{-O}). That has several consequences for channel gating, some of which are not intuitively obvious. For α II, the C_4 -O equilibrium favors C_4 at -60 mV and below, and, even at more positive voltages, a significant fraction of channels remain closed. This contributes to the positive shift in the voltage dependence of activation for α II. It also allows more closed-state inactivation, since the C_4 and C_3 states are assumed to inactivate as rapidly as O.

How does the model produce the three exponential components of tail currents? At -40 mV, channel closing is much faster than inactivation ($k_{-O} = 324$ s $^{-1}$ and $k_I = 7$ s $^{-1}$), and the C-C rates are intermediate (14–160 s $^{-1}$). Both the C-O equilibrium, and the equilibrium for activation of an individual voltage sensor, favor activation slightly. During a tail current, a fraction of the channels move rapidly from O to C_4 ; next, slower C-C transitions pull more channels away from the open state; finally, inactivation pulls the remaining channels away from the open and closed states. A large fraction of channels transiently accumulates in closed states, but at steady state, nearly all of the channels are inactivated. On a 500-ms time scale, three exponentials were required to fit tail currents simulated from the model at -40 mV ($\tau = 1.3, 23,$ and 160 ms, with nearly equal amplitudes). The three time constants correspond closely to the kinetics of the O-C, C-C, and C-I transitions.

Why are three exponential components not apparent for α IG tail currents? First, the channel closing rate is

much closer to the inactivation rate (at -40 mV $k_{-O} = 81$ s $^{-1}$ and $k_I = 70$ s $^{-1}$), so closing and inactivation occur on the same time scale. In addition, the C-O equilibrium is strongly to the right for α IG, by about a factor of 50 at -40 mV. This means that most channels that inactivate do so directly from the open state (α II channels tend to close first). The C-O equilibrium also makes the net rate of channel closing much slower than k_{-O} . As a result, with the parameters used for α IG, the model predicts tail currents that are described almost perfectly by single exponentials. This can be attributed entirely to the difference in channel closing rate between α IG and α II, relative to the other rate constants in the models. For α II, when k_{-O} at 0 mV was changed from 100 to 3 s $^{-1}$ (eightfold slower than α IG, versus fourfold faster), tail currents were effectively monoexponential over a wide voltage range (unpublished data).

Some features of the data were not described well by the model for α II. In particular, there was no slow component of inactivation. Presumably, that reflects a separate slow inactivation mechanism, which is not included in the model. Thus, the model should be considered to apply primarily to α II kinetics on the <1 -s time scale. In addition, although the model produced clearly biexponential tail currents on a 50-ms time scale (Fig. 12 D), and the two time constants were close to the experimental values (Fig. 3), the relative amplitudes of the two components were not well reproduced (note the large amplitude of slow deactivation at -60 mV in Fig. 13 C versus Fig. 11 C). Also, the model did not predict the change in relative amplitudes of fast and slow deactivation with partial inactivation (Fig. 4, C and D), so that effect could result from a kinetic process not included in the model (e.g., facilitation; Klöck-

ner et al., 1999). Overall, we view this model as an illustration of one possible mechanism for gating of α II, rather than as a complete quantitative description.

DISCUSSION

Our goal was to compare the gating kinetics of the α II calcium channel to α IG, which exhibits more “typical” T-channel kinetics, using whole-cell recording and kinetic modeling. The starting point was the observation that α II activates and inactivates more slowly than α IG. Mechanistically, those two differences could be explained either by slower microscopic inactivation or by slower microscopic activation. If activation is slow and rate-limiting for macroscopic inactivation (Aldrich et al., 1983), slower activation can produce slower macroscopic inactivation, even if activation and inactivation are only partially coupled (Carbone and Lux, 1987). Alternatively, slower inactivation will appear to slow activation, as activation continues longer, allowing more channels to activate (Gonoi and Hille, 1987).

To fully explain our results, we found that both activation and inactivation had to be slower for α II. Slower activation is not sufficient, as inactivation becomes voltage-independent above -50 mV, suggesting that microscopic inactivation is rate-limiting. Note also that the activation rate and the time to peak accelerate at least 10-fold with depolarization above -50 mV, which is further evidence that activation is not rate-limiting for inactivation in that region. On the other hand, if only microscopic inactivation is slowed, the slow activation and deactivation kinetics observed near -40 mV (Fig. 5 A) would not occur. However, gating of α II is not uniformly slower than α IG, since deactivation is faster for α II at strongly hyperpolarized voltages (Fig. 3). A quantitative difference in the channel closing rate produced qualitative differences in kinetic behavior, most notably multiexponential tail currents for α II.

Gating Kinetics of α II

Several basic features of gating of α II agree with previous studies. Compared with α IG and most other T-channels, activation and inactivation are slow, but deactivation is fast (Kozlov et al., 1999; Lee et al., 1999; Monteil et al., 2000; McRory et al., 2001).

We find a more positive activation curve ($V_{1/2} = -20$ mV) than most previous studies ($[-44$ mV] Klöckner et al., 1999; $[-41$ mV] Monteil et al., 2000; $[-61$ mV] McRory et al., 2001), although Lee et al. (1999) found $V_{1/2} = -25$ mV. Some of the variation could result from surface charge effects, as different concentrations of Ca^{2+} or Ba^{2+} have been used as charge carriers. One key difference is that previous studies used conductances (rather than $P_{O,r}$), which would affect the shape of the activation curve since the open-channel I-V is nonlinear

(Fig. 1 C). In addition, we find that α II channels continue to activate at positive potentials (Fig. 1 D), whereas most previous studies of activation were based primarily on data at negative voltages. If we use chord conductances rather than $P_{O,r}$, and fit only to $+10$ mV, a single Boltzmann gives an apparent $V_{1/2} = -43$ mV. The chord conductances are affected not only by the channel open probability, but also by the voltage dependence of the open-channel current, so that $V_{1/2}$ does not accurately describe the voltage dependence of channel opening.

Although we were unable to reach steady-state inactivation without evoking slow inactivation, we would estimate from Fig. 7 that fast inactivation is half complete near -70 mV. This agrees well with several previous studies (Klöckner et al., 1999; Lee et al., 1999; Monteil et al., 2000), although we would expect that the 5–15-s steps used previously would produce some amount of slow inactivation. In contrast, McRory et al. (2001) found a $V_{1/2}$ of -93 mV for α II using 15-s pulses. The kinetic differences observed by McRory et al. (2001) may be related to sequence differences in their rat α II clone (as described in MATERIALS AND METHODS).

Some kinetic parameters varied significantly among cells. For example, in one set of 16 cells, the time constant for inactivation during 600-ms steps to -20 mV was 147 ± 9 ms (SD = 37 ms). In cells tested at both -20 and $+60$ mV, inactivation rates were similar, so the variability does not result from the voltage dependence of inactivation. Inactivation time constants could vary twofold for cells recorded on the same day, with no obvious explanation. Such variability could contribute to the quantitative differences among previous studies of α II kinetics, and might also indicate that α II gating can be regulated by, as yet, unknown factors.

One striking difference from previous studies on α II is our observation that tail currents are bi- or even triexponential. It is not clear why this was not observed previously, although we appear to have examined a wider voltage range and longer time scale than in some other studies.

The kinetics of α II are similar in several respects to the T-current of thalamic reticular neurons (Huguenard and Prince, 1992). In those cells, time constants were 80–100 ms for inactivation (from -20 to -50 mV) and 500–700 ms for recovery (from -100 to -80 mV), and activation kinetics were shifted by ~ 10 mV to more positive voltages, compared with the more classical T-current of thalamic relay neurons. Combined with the high level of expression of α II in thalamic reticular neurons (Talley et al., 1999), it seems likely that α II makes a major contribution to the T-current in those cells.

Gating Mechanisms of α II

Activation and inactivation of α II can be described by an allosteric model, where voltage-dependent activation

is coupled to an intrinsically voltage-independent inactivation process (Figs. 12–13). The same model, but with substantially different parameters (Table I), was previously used to describe $\alpha 1G$ (Serrano et al., 1999).

Several features of gating of $\alpha 1I$ do qualitatively resemble $\alpha 1G$. Inactivation is strong, but only 98–99% complete, even with strong depolarization. The macroscopic time constants for inactivation and recovery reach limiting rates at positive and negative voltages, respectively. It is especially striking that inactivation is nearly voltage-independent over a wide range (-30 to $+70$ mV) for both channels. Only in a narrow voltage region do the time constants for inactivation and recovery exhibit the voltage dependence expected from coupling to the activation process (Fig. 3). This appears to result from a relatively weak allosteric coupling, such that the inactivation and recovery rates do not vary dramatically with the state of the channel, although the coupling is strong enough to produce the observed voltage dependence of inactivation. A similar point was made recently by Kuo and Yang (2001), who reported that recovery from inactivation was not detectably voltage dependent for T-currents of thalamic neurons.

For both $\alpha 1G$ and $\alpha 1I$, our models assume that inactivation is as fast from certain closed states (Fig. 12 A, C_3 and C_4) as from the open state itself. For $\alpha 1G$, that assumption was made merely to improve the quality of the fit to the data. For $\alpha 1I$, we present more direct evidence: inactivation is as fast at -20 mV as at $+60$ mV, even though $P_{O,r}$ is considerably lower at -20 mV (Fig. 1 D versus Fig. 3; Fig. 11, C and D). In retrospect, that argument also holds for $\alpha 1G$, since the inactivation rate reached a limiting value by -30 mV, where only 70% of the channels were activated (Serrano et al., 1999).

$\alpha 1I$ clearly differs from $\alpha 1G$ in the absolute rates of activation and inactivation. More significantly, there were two apparent qualitative differences between the two channels, with $\alpha 1G$ exhibiting monoexponential tail currents and less closed-state inactivation at positive voltages (Serrano et al., 1999). We propose that both effects result from a faster channel closing rate for $\alpha 1I$. In our model, that rate is fourfold faster for $\alpha 1I$ in absolute terms, and 20–50-fold faster relative to the other rate constants in the model.

Slow inactivation on a time scale of seconds or minutes appears to be a nearly universal property of channels that also exhibit a fast inactivation process. We find slow inactivation for $\alpha 1I$ on the 1–10-s time scale (Fig. 9), and a preliminary report has appeared of slow inactivation for $\alpha 1G$ (Hering et al., 2001). We did not find evidence for slow inactivation for $\alpha 1G$ (Serrano et al., 1999), probably because we intentionally limited that study to depolarizations lasting 1 s or less. Biexponential inactivation and recovery has been reported previ-

ously for some native T-channels (Bossu and Feltz, 1986; Herrington and Lingle, 1992).

The molecular basis of T-channel inactivation remains to be determined. Some features resemble Na^+ channels more closely than other Ca^{2+} channels; at the level of amino acid sequence, T-channels are only slightly closer to other Ca^{2+} channels than to Na^+ channels. But there is no clear homology between T-channels and Na^+ channels in the III-IV linker, which is critical for inactivation of Na^+ channels. It will also be important to find the molecular determinants of the differences in activation and inactivation kinetics among T-type channels.

This work was supported in part by National Institutes of Health grants (NS24471) to S.W. Jones and (NS38691) E. Perez-Reyes, an NIH postdoctoral fellowship (NS10828) to C.J. Frazier, and a Howard Hughes Medical Institute grant to Case Western Reserve University School of Medicine.

Submitted: 17 July 2001

Revised: 4 September 2001

Accepted: 4 September 2001

REFERENCES

- Aldrich, R.W., D.P. Corey, and C.F. Stevens. 1983. A reinterpretation of mammalian sodium channel gating based on single channel recording. *Nature*. 306:436–441.
- Armstrong, C.M., and D.R. Matteson. 1985. Two distinct populations of calcium channels in a clonal line of pituitary cells. *Science*. 227:65–67.
- Armstrong, C.M., and F. Bezanilla. 1977. Inactivation of the sodium channel. II. Gating current experiments. *J. Gen. Physiol.* 70:567–590.
- Bean, B.P. 1981. Sodium channel inactivation in the crayfish giant axon. Must channels open before inactivating? *Biophys. J.* 35:595–614.
- Bossu, J.L., and A. Feltz. 1986. Inactivation of the low-threshold transient calcium current in rat sensory neurones: evidence for a dual process. *J. Physiol.* 376:341–357.
- Brooks, S.P., and K.B. Storey. 1992. Bound and determined: a computer program for making buffers of defined ion concentrations. *Anal. Biochem.* 201:119–126.
- Brown, A.M., Y. Tsuda, and D.L. Wilson. 1983. A description of activation and conduction in calcium channels based on tail and turn-on current measurements in the snail. *J. Physiol.* 344:549–583.
- Carbone, E., and H.D. Lux. 1984. A low voltage-activated, fully inactivating Ca channel in vertebrate sensory neurones. *Nature*. 310: 501–502.
- Carbone, E., and H.D. Lux. 1987. Single low-voltage-activated calcium channels in chick and rat sensory neurones. *J. Physiol.* 386: 571–601.
- Coulter, D.A., J.R. Huguenard, and D.A. Prince. 1989. Calcium currents in rat thalamocortical relay neurones: kinetic properties of the transient, low-threshold current. *J. Physiol.* 414:587–604.
- Cribbs, L.L., J.H. Lee, J. Yang, J. Satin, Y. Zhang, A. Daud, J. Barclay, M.P. Williamson, M. Fox, M. Rees, and E. Perez-Reyes. 1998. Cloning and characterization of $\alpha 1H$ from human heart, a member of the T-type Ca^{2+} channel gene family. *Circ. Res.* 83:103–109.
- Frazier, C.J., E.G. George, and S.W. Jones. 2000. Apparent change in ion selectivity caused by changes in intracellular K^+ during whole-cell recording. *Biophys. J.* 78:1872–1880.
- Gonoi, T., and B. Hille. 1987. Gating of Na channels. Inactivation

- modifiers discriminate among models. *J. Gen. Physiol.* 89:253–274.
- Hering, J., Y. Maulet, A. Feltz, and R.C. Lambert. 2001. Slow inactivation of the CaV3.1 isoform of the T type calcium channel. *Biophys. J.* 80:621A–622A (*Abstr.*).
- Herrington, J., and C.J. Lingle. 1992. Kinetic and pharmacological properties of low voltage-activated Ca²⁺ current in rat clonal (GH₃) pituitary cells. *J. Neurophysiol.* 68:213–232.
- Huguenard, J.R. 1996. Low-threshold calcium currents in central nervous system neurons. *Annu. Rev. Physiol.* 58:329–348.
- Huguenard, J.R., and D.A. McCormick. 1992. Simulation of the currents involved in rhythmic oscillations in thalamic relay neurons. *J. Neurophysiol.* 68:1373–1383.
- Huguenard, J.R., and D.A. Prince. 1992. A novel T-type current underlies prolonged Ca²⁺-dependent burst firing in GABAergic neurons of rat thalamic reticular nucleus. *J. Neurosci.* 12:3804–3817.
- Klößner, U., J.H. Lee, L.L. Cribbs, A. Daud, J. Hescheler, A. Pervezzev, E. Perez-Reyes, and T. Schneider. 1999. Comparison of the Ca²⁺ currents induced by expression of three cloned $\alpha 1$ subunits, $\alpha 1G$, $\alpha 1H$ and $\alpha 1I$, of low-voltage-activated T-type Ca²⁺ channels. *Eur. J. Neurosci.* 11:4171–4178.
- Kozlov, A.S., F. McKenna, J.H. Lee, L.L. Cribbs, E. Perez-Reyes, A. Feltz, and R.C. Lambert. 1999. Distinct kinetics of cloned T-type Ca²⁺ channels lead to differential Ca²⁺ entry and frequency-dependence during mock action potentials. *Eur. J. Neurosci.* 11:4149–4158.
- Kuo, C.-C., and B.P. Bean. 1994. Na⁺ channels must deactivate to recover from inactivation. *Neuron.* 12:819–829.
- Kuo, C.C., and S. Yang. 2001. Recovery from inactivation of T-type Ca²⁺ channels in rat thalamic neurons. *J. Neurosci.* 21:1884–1892.
- Lee, J.H., A.N. Daud, L.L. Cribbs, A.E. Lacerda, A. Pervezzev, U. Klößner, T. Schneider, and E. Perez-Reyes. 1999. Cloning and expression of a novel member of the low voltage-activated T-type calcium channel family. *J. Neurosci.* 19:1912–1921.
- McRory, J.E., C.M. Santi, K.S. Hamming, J. Mezeyova, K.G. Sutton, D.L. Baillie, A. Stea, and T.P. Snutch. 2001. Molecular and functional characterization of a family of rat brain T-type calcium channels. *J. Biol. Chem.* 276:3999–4011.
- Monteil, A., J. Chemin, V. Leuranguer, C. Altier, G. Mennessier, E. Bourinet, P. Lory, and J. Nargeot. 2000. Specific properties of T-type calcium channels generated by the human α_{1I} subunit. *J. Biol. Chem.* 275:16530–16535.
- Perez-Reyes, E., L.L. Cribbs, A. Daud, A.E. Lacerda, J. Barclay, M.P. Williamson, M. Fox, M. Rees, and J.H. Lee. 1998. Molecular characterization of a neuronal low-voltage-activated T-type calcium channel. *Nature.* 391:896–900.
- Serrano, J.R., E. Perez-Reyes, and S.W. Jones. 1999. State-dependent inactivation of the $\alpha 1G$ T-type calcium channel. *J. Gen. Physiol.* 114:185–201.
- Serrano, J.R., S.R. Dashti, E. Perez-Reyes, and S.W. Jones. 2000. Mg²⁺ block unmasks Ca²⁺/Ba²⁺ selectivity of $\alpha 1G$ T-type calcium channels. *Biophys. J.* 79:3052–3062.
- Talley, E.M., L.L. Cribbs, J.H. Lee, A. Daud, E. Perez-Reyes, and D.A. Bayliss. 1999. Differential distribution of three members of a gene family encoding low voltage-activated (T-type) calcium channels. *J. Neurosci.* 19:1895–1911.
- Warre, R., and A. Randall. 2000. Modulation of the deactivation kinetics of a recombinant rat T-type Ca²⁺ channel by prior inactivation. *Neurosci. Lett.* 293:216–220.